LANGMUIR

pubs.acs.org/Langmuir
Article

Unexpected Behavior of Streaming Potential in Ion-Exchange Membranes

Wouter Badenhorst, Kuldeep, Jose Antonio Manzanares, and Lasse Murtomäki*

Cite This: https://doi.org/10.1021/acs.langmuir.4c00027
Read Online

ABSTRACT: Streaming potential is one of the numerous electrokinetic phenomena created when an electrolyte flows along a charged surface. In membranes, applying the charged cylindrical pore model, streaming potential can be used to estimate, e.g., the pore size and the charge density of such pores. In this study, we are extending streaming potential experiments to ion-exchange membranes (IEMs) and trying to verify the existing models with the measurements. According to the Donnan equilibrium between an electrolyte solution and an IEM, the solution concentration should not affect the streaming potential if the membrane charge is even moderately low. Yet, the streaming potential varied substantially with the solution concentration, as in the case of nearly neutral porous membranes. In addition, the existing theory does not include the membrane thickness, but we found that thinner membranes showed larger streaming potentials. These dilemmas are discussed in this paper.

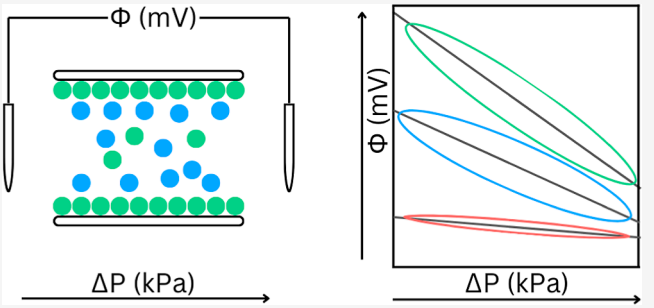

INTRODUCTION

Ion-exchange membranes (IEMs) are used in various applications in different fields such as water purification and desalination, membrane separation processes, chlor-alkali industry, electrodialysis, fuel cells, batteries, etc.[1−4] The functionality of IEMs is based on their permselectivity due to fixed-charge groups that are covalently bound to the membrane matrix. It has long been known that the transport of electric charge across an IEM is coupled to the transport of the volume. Electroosmosis was discovered by Reuss in 1809, and streaming potential was first observed by Quincke in 1859. Streaming potential measurements are insightful for membrane characterization as they elucidate relationships between membrane structure [morphology, porosity, and ion-exchange capacity (IEC)] and function.[5,6] Also remarkable have been the studies on the adsorption of charged species in biological and synthetic membranes using streaming potential.[7−12]

When we consider a system composed of two identical electrolyte solutions (left L and right R) separated by a membrane, the coupled volume and electric charge flows are described by the phenomenological transport equations

$$J_V = L_{11}\Delta P + L_{12}\Delta\phi \tag{1}$$

$$I = L_{21}\Delta P + L_{22}\Delta\phi \tag{2}$$

where J_V and I are the volume flow and the electric current, respectively, $\Delta P = P^L - P^R$ is the pressure difference, $\Delta\phi = \phi^L - \phi^R$ is the electric potential difference, L_{11} is the hydraulic permeability of the membrane, and L_{22} is its electrical conductance. In an electroosmosis experiment, we have $\Delta P = 0$ and $J_V = L_{12}\Delta\phi = (L_{12}/L_{22})I$.[5,7,13−15] In a streaming potential experiment, we have $I = 0$ and $\Delta\phi = -(L_{21}/L_{22})\Delta P$. The streaming potential is defined as

$$\nu \equiv \left(\frac{\Delta\phi}{\Delta P}\right)_{I=0} = -\frac{L_{21}}{L_{22}} \tag{3}$$

Streaming potential measurements are important because they provide the most accurate determinations of the phenomenological cross coefficient L_{21}.[16] Concentration polarization develops when an electric current passes through an IEM that separates two identical electrolyte solutions. Thus, in electro-osmosis experiments across IEMs, the cross coefficient L_{12} is affected by the concentration gradients in the diffusion boundary layers. Concentration polarization also develops when an applied pressure gradient generates the flow of electrolyte solution through an IEM because its permselectivity implies a reduced electrolyte permeability. However, concentration polarization is weaker in streaming potential experiments, and it can be avoided by analyzing the initial values of the streaming potential just after the onset of the applied pressure difference. Hence, the experimentally determined cross coefficients L_{12} and L_{21} are similar to each

Received: January 3, 2024
Revised: March 13, 2024
Accepted: March 13, 2024

other but not exactly equal.[16] To avoid the concentration polarization effects, some authors determine the electro-osmosis cross coefficient L_{12} from the cross coefficient L_{21} in streaming potential, assuming the reciprocity relation $L_{12} = L_{21}$.[17]

The thermodynamic-phenomenological equations for the coupled transport of volume and electric charge are local. The flux densities of charge and volume are expressed as linear combinations of the local gradients of the pressure and electric potential. The cross coefficients in the local transport equations satisfy the Onsager reciprocal relation. In charged capillaries, this relation can be proved theoretically from the Navier−Stokes and Poisson equation.[18] In theory, eqs 1 and 2 are obtained by integration of the local transport equations from the bulk L solution to the bulk R solution.[19] The phenomenological coefficients L_{ij} depend on the actual distribution of electric potential, water and ionic species concentrations, and solution velocity across the system.

Theoretical expressions for the streaming potential were first obtained from the Kedem−Katchalsky treatment.[7,9,16,20] The extension of the Teorell−Meyer−Sievers (TMS) model to incorporate the effect of the pressure gradient using linear irreversible thermodynamics led to the expression

$$|\nu| = \frac{RT}{F}\frac{a^2}{8\eta D_1}\frac{1}{1 + 2(c^b/X)^2} \tag{4}$$

where c^b is the 1:1 electrolyte concentration in the external solutions,[13] X is the concentration of fixed-charge groups in the membrane (referred to as the volume of solution in the membrane pores), R is the molar gas constant, F is Faraday constant, T is the thermodynamic temperature, and η is the dynamic viscosity of the solution. It is apparent from eq 4 that, in the limit of low concentrations $c^b \ll X$, the streaming potential of IEMs is expected to reach a limiting value $|\nu_\infty| \equiv a^2RT/8F\eta D_1$ that depends on the effective radius a of the membrane pores and the counterion diffusion coefficient D_1, and is independent of X.[21]

With the development of the capillary space-charge model (SCM),[8,20] the theoretical calculations provided more physical insights on the relation between the streaming potential of IEMs and the radial distributions of electric potential, ionic concentrations, and solution velocity.[9,19] However, both the SCM and the TMS models incorporate as a basic assumption the rigidity of the membrane structure. That is, while the theoretical calculations invariably assume constant effective pore radius a and constant fixed-charge concentration X, these parameters are related to the membrane water content so that an increase in water content (due to, e.g., membrane swelling at low electrolyte concentration) results in a larger effective a and lower X. Therefore, these theoretical predictions can only be in qualitative agreement with the experimental results.[13,17]

Due to the delicacy of the measurement techniques, it is difficult to find reliable data on the streaming potential of IEMs.[22] The tendency to the limiting value $|\nu_\infty|$ of the streaming potential at very low concentrations, eq 4, has been observed in some studies but not so clearly in others.[17,22,23] Moreover, when using trivalent counterions, this limiting behavior is not observed.[17]

Although other characteristics of the IEMs also affect their streaming potential ν, most studies conclude that the streaming potential is higher for membranes with higher water content.[17,22] Trivijitkasem and Østvold[17] measured the streaming potential of commercially available, strongly charged cation- and anion-exchange membranes, and determined the water transport number in the membranes.[22] They observed that for monovalent and multivalent electrolytes, streaming potential increased with increasing water content of the membranes. Their observations were in agreement with the limiting value $|\nu_\infty| = a^2RT/8F\eta D_1$. Also, the streaming potential became constant for very low external electrolyte concentrations. The observed limiting streaming potential was not affected by a change of co-ion but was affected by the change of the counterion, in agreement with the theoretical prediction $|\nu_\infty| \propto 1/D_1$, i.e., inversely proportional to the counterion diffusion coefficient. Agreement with $|\nu_\infty| \propto 1/D_1$ was also observed by Toyoshima and Nozaki and Reynard et al.[22,23]

When increasing the electrolyte concentration, it is expected that co-ion exclusion is poorer, the membrane permselectivity decreases, and streaming potential decreases in magnitude. For homogeneous membranes, the Donnan theory predicts that the decrease in permselectivity and streaming potential with increasing c^b occurs when $c^b \approx X$, as described by eq 4. However, experimental observations evidence that the decrease occurs at significantly lower electrolyte concentrations.[17,22−25] These observations are likely related to the fact that any inhomogeneity in the distribution of fixed-charge groups leads to poorer co-ion exclusion than predicted by Donnan theory and to changes in membrane swelling with external electrolyte concentration.[26−28]

Trivijitkasem and Østvold observed that the magnitude of the streaming potential became smaller than $|\nu_\infty|$ when the electrolyte concentration exceeded about 0.01 mol/L.[17] Also it was noticed that the measured streaming potential was independent of the nature of the co-ions even at 1 mol/L external concentration, even though a significant co-ion concentration would then be expected in the membrane pores. Their results with mono-, di-, and trivalent counterions at the lowest concentrations indicated that streaming potential is typically lower for monovalent, intermediate for divalent, and larger for trivalent counterions, as it could be expected from eq 4 and their diffusion coefficients. The values observed with trivalent counterions were somehow larger than those predicted by eq 4. These authors attributed this observation to a larger hydration number.

Somovilla et al. determined streaming potentials in 10 mM NaCl and the water content (or liquid uptake) of five commercial sulfonated cation-exchange membranes.[5] When membranes of equal character (homogeneous/heterogeneous) were compared, they found that there seems to be a relation between the streaming potential and the fixed-charge concentration because they claimed that higher fixed-charge concentrations lead to higher electrokinetic coefficients. They also found that the streaming potential was larger in heterogeneous membranes (such as MK-40 and CR65-CZL-412) than that in homogeneous membranes (such as Nafion 115). This was in agreement with previous results showing that membranes with higher water content or higher degree of swelling have higher streaming potentials[22] because heterogeneous membranes exhibit higher liquid content than homogeneous membranes. However, the Nafion 115 membrane did not follow this trend as it had the largest magnitude of the streaming potential and the lowest water content. For instance, the streaming potential of the Nafion 115 membrane was reported as about three times higher than that of the MK-

https://doi.org/10.1021/acs.langmuir.4c00027
Langmuir XXXX, XXX, XXX−XXX

40 membrane. Yet, the water content and wet porosity of MK-40 were estimated as about 2.7 and 1.3 times higher than those of Nafion 115, respectively. In addition, the MK40 membrane was about 3.7 times thicker than the Nafion 115 membrane. They speculated that the large streaming potential of the Nafion 115 membrane could be attributed to a structural effect. In any case, the streaming potential seems to be affected by a combined effect of membrane thickness, porosity, and water content.

The streaming potential in porous membranes (Millipore, Durapore, Cyclopore, Nuclepore, etc.) does not tend to the limiting value $|\nu_\infty|$.[10,29,30] On the contrary, it usually increases with decreasing external solution concentration, and high values of the order of several μV/Pa can easily be measured below 0.1 M.[10,29] In some porous membranes, a maximum of streaming potential vs external concentration was observed in the range 2−5 mM. The value of the maximum was proportional to the pore radius and appeared at concentrations that decreased with increasing pore radius.[30] These observations were explained on the basis of the SCM and the dependence of the surface charge with concentration, as described by the Freundlich adsorption isotherm.[9,30]

In this article, we report measurements of the streaming potential of commercially available IEMs and some porous membranes (Millipore, Daramic). Also, we modified Daramic with sulfonated polyether−ether−ketone (S-PEEK) to prepare an inexpensive alternative for commercial cation-exchange membranes. We study the dependence of the streaming potential on the solution concentration, both experimentally and theoretically. We also study experimentally the effect of the membrane thickness on the streaming potential and discuss the reasons that the current theory does not describe this observed effect.

EXPERIMENTAL SECTION

Materials. Polyether−ether−ketone powder, dimethyl sulfoxide, and sulfuric acid (95−98% mass fraction) were obtained from Sigma-Aldrich. KCl (99.0%, Merck BioXtra, Germany) was used as received. Commercially available membranes and separators such as Nafion N115 (Ion-Power GmbH), Millipore (type VVHP 0.1 μm), microporous Daramic separator, anion-exchange membrane AR103P (Veolia, formerly SUEZ, Water Technologies & Solutions), and cation-exchange membranes CR61N and CR61P (Veolia Water Technologies & Solutions) were used. In addition, S-PEEK (10%)-Daramic was synthesized at laboratory premises. All membranes and separators (Table 1) are subjected to a soak treatment in a 2 M KCl solution for 2 days. Afterward, they are allowed to equilibrate in an electrolyte concentration measurement setup for 2 days.

Preparation of S-PEEK Membranes. To produce the sulfonated polyether−ether−ketone, we initiated the process by adding 10 g of polyether−ether−ketone powder to 100 mL of 95−98% H_2SO_4, which had been heated to 60 °C. This reaction took place in a three-necked flask and was facilitated by mechanical agitation using a magnetic stirrer. The agitation was sustained for 4 h, resulting in an approximate sulfonation degree of 67%, as corroborated by prior findings reported by Xi et al.[31] Once sulfonation was deemed complete, the solution, now containing S-PEEK, was carefully transferred into a container filled with an excess of ice water. This step induced the precipitation of S-PEEK, while simultaneously diluting sulfuric acid, effectively terminating the sulfonation process.

The newly formed solid S-PEEK was subjected to successive filtration steps until the effluent reached a pH of 7. Subsequently, the S-PEEK underwent vacuum drying at 60 °C for 24 h. To create the casting solution, we dissolved the S-PEEK in an appropriate quantity of dimethylformamide until a solution with an S-PEEK mass fraction of 10% was achieved. This solution was stirred for 24 h, followed by filtration and a final step of sonication for 30 min to eliminate any trapped gases within the casting solution. For the casting process, 0.5 mL of the solution was dispensed onto a Daramic substrate (a porous polyethene separator with a thickness of 0.6 mm) and allowed to air-dry in a fume hood. Subsequently, the casting was further vacuum-dried at 60 °C for 24 h.

Streaming Potential Setup. The geometry of the measurement cell is presented in our earlier papers.[10−12] The cell allows for the in and out flow of electrolytes, connection to a differential pressure sensor, and insertion of Ag|AgCl reference electrodes (Figure 1). Furthermore, the cell allows for reverse osmosis netting with 2 × 2 mm grids and a 2 mm thickness to prevent the membrane from bending when the system is under pressure. The membrane is secured between the two-halves of the cell, sealed using 2 mm thick silicone gaskets on either side, and compressed using M4 bolts in each corner.

A schematic representation of the streaming potential setup is shown in Figure 1. The operational amplifier circuit used an OPA2191 precision operational amplifier (Texas Instruments) in an instrumentation amplifier configuration. The circuit was operated using two 9 V batteries together with a LM78M05 precision +5 V regulator and a L790SCV −5 V regulator (STMicroelectronics) together with the manufacturer-recommended capacitors for clean power delivery to the precision operational amplifiers. The voltages from the amplifier circuit were fed into an ADS 1115 16-bit analog-to-digital converter (ADC, Adafruit) and an RP-2040 microcontroller running Circuit Python and read with no further gain. The outputs from the OPA2191s were level-shifted by 2.5 V using a precision voltage reference (ADR03, Analog Devices) to prevent negative voltages from being supplied to the ADS 1115. Suitable gain could be set for each of the experiments by adjusting the gain resistor in the OPA2191 instrumentation amplifier configuration. The differential pressure of the system was read using a 6CF6D differential pressure sensor (Honeywell) and was powered and read using a NAU7802 24-bit ADC (Adafruit), and the pressure readings were recorded using an RP-2040 microcontroller.

For calibration curve data of the pressure sensor, a typical manometer setup was employed. Voltage calibration was performed using a Keithley 2420 source meter unit, through applying a known current over a precision 1 Ω resistor, and was done to account for resistor mismatches. Control software (written in Python) both operated an Ismatec peristaltic pump via a NI-6215 DAQ and the analog control inputs available on the Ismatec pump and recorded the pressure and voltage measurements obtained from the RP-2040 microcontroller (Cytron Maker Pi RP2040).

Table 1. Properties of the Membranes Used in This Study[a]

membrane	thickness (μm)	porosity (%)	pore size (μm)	WU (%)	IEC (mequiv/g)
Millipore	125	70	0.10		
CR61N	300			44	2.2
CR61P	580			44	2.2
AR103P	570			39	2.37
Daramic	350	58	0.15		
S-PEEK	350			38	1.91
N115	127			38	0.95

[a]Values provided by the supplier and earlier publications.[2,31−34]

RESULTS AND DISCUSSION

The results of streaming potential $\Delta\phi/\Delta P$ measurements in the KCl electrolyte are collected in Table 2. The first observation is that in all cases, the streaming potential depends on the KCl concentration, which is not expected for IEMs. Neutral separators (Millipore and Daramic) show negative values, which is due to chloride adsorption, as we have seen earlier.[11] Daramic has bigger pore size than Millipore (Table 1) and, hence, higher streaming potential (Table 2).[7]

https://doi.org/10.1021/acs.langmuir.4c00027
Langmuir XXXX, XXX, XXX−XXX

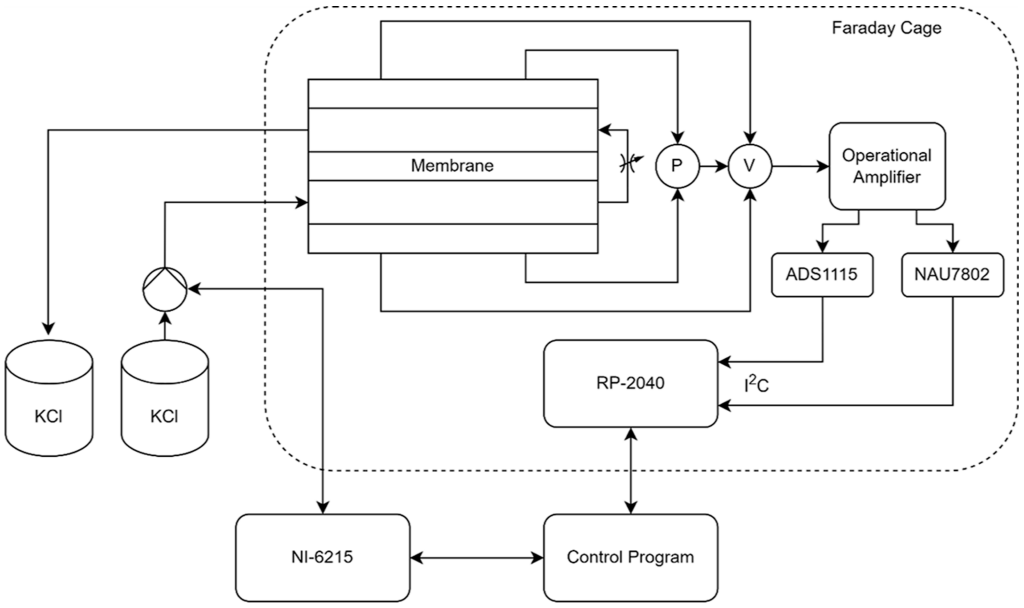

Figure 1. Schematic representation of the streaming potential setup used.

Table 2. Streaming Potential in nV/Pa of Various Membranes at Differing KCl Concentrations

KCl (mM)	Millipore	CR61N	CR61P	AR103P	Daramic	S-PEEK	N115
1	−629	−55.3	−5.2	16.40	−1830	−54.8	−30.2
10	−209.2	−20.19	−3.7	6.26	−621	−13.3	−14.8
100	−42.8	−1.26	−0.94	2.85	−208	−1.3	−4.2

Modifying Daramic with S-PEEK adds negative charges to the membrane, closing its pores and decreasing the streaming potential accordingly.

Commercial IEMs CR61P and AR103P are relatively similar to each other concerning their thickness and IEC, but the latter anion-exchange membrane shows significantly higher streaming potential (in absolute value), which manifests the fact that co-ion exclusion is weaker in anion-exchange membranes than that in cation-exchange membranes. Interestingly, the streaming potential of Nafion N115 compares with that of CR61N. The latter is a much thicker cation-exchange membrane with double IEC than N115, and both have similar water uptakes (see WU in Table 1) The streaming potential is expected to increase with increasing IEC (see Figure 1b in the Appendix) and to decrease with increasing membrane thickness. These opposing effects seem to compensate each other and result in similar streaming potential for CR61N and Nafion N115.

The effect of the membrane thickness is shown in Table 2. The two chemically identical membranes CR61P and CR61N, with the thickness of 580 and 300 μm, respectively, show significantly different streaming potentials, yet approaching each other at higher KCl concentrations.

As mentioned above, CR61N is comparable with Nafion N115, although its thickness is 2.5-fold that of Nafion N115. S-PEEK-modified Daramic has characteristics very similar to CR61N and, consequently, its streaming potential is very close to that of CR61N. The effect of thickness on the hysteresis is evident in Figure 2c. Hysteresis appears as a consequence of concentration polarization on both sides of the membrane. A brief description of the formation of the concentration polarization is given in the Appendix. Concentration polarization affects both the electric potential difference and the effective pressure difference. The electric potential difference then has a diffusion potential contribution, but this is small and does not explain the hysteresis. The driving force for solution flow is $\Delta P - \Delta\Pi$, where $\Delta\Pi = 2RT\Delta c$ is the osmotic pressure difference that appears due to concentration polarization (for a symmetric, strong electrolyte).[35] The concentrations at the external membrane boundaries can be roughly estimated as $c(0) = c^{b}e^{Pe}$ and $c(L) = c^{b}e^{-Pe}$, where Pe is the Peclet number in the diffusion boundary layers (see the Appendix). A typical value of Peclet number can be $Pe \approx 0.05$, which roughly means that the concentration polarization is of the order of 5%. Thus, for $c^{b} = 10$ mM, we can estimate that $\Delta\Pi = 4RTc^{b} \sinh Pe \approx 5$ kPa, which is in agreement with the pressure difference (at constant $\Delta\phi$) that is observed in Figure 2c between the experimental points and the linear fit.

The theory included in the Appendix predicts that streaming potential would be inversely proportional to the product of charge number and diffusion coefficient of the counterion, z_1D_1. The order of this product in aqueous solutions is $K^+ > Ca^{2+} > Na^+$, in agreement with the observations in Table 3 and Figure 3. This agreement suggests that the values of the diffusion coefficients of these cations inside the CR61N membrane are on the same order as in bulk solution at infinite dilution.

The order of magnitude of streaming potential in all of our measurements is 1 nV/Pa, so that extremely stable electrodes are required. At these low values of ν, the correction for the electrode potentials concerning pressure might be appropriate. As Spiegler has shown, the correction for $\Delta\nu$ would be

$$\Delta\nu = (V_{AgCl} - V_{Ag} - V_{Cl^-})/F \quad (5)$$

where V_i is the partial molar volume of the species i.[36] Using their literature values, the correction is 0.067 nV/Pa, i.e., not completely insignificant, yet only 5% in our "worst" case. The

https://doi.org/10.1021/acs.langmuir.4c00027
Langmuir XXXX, XXX, XXX−XXX

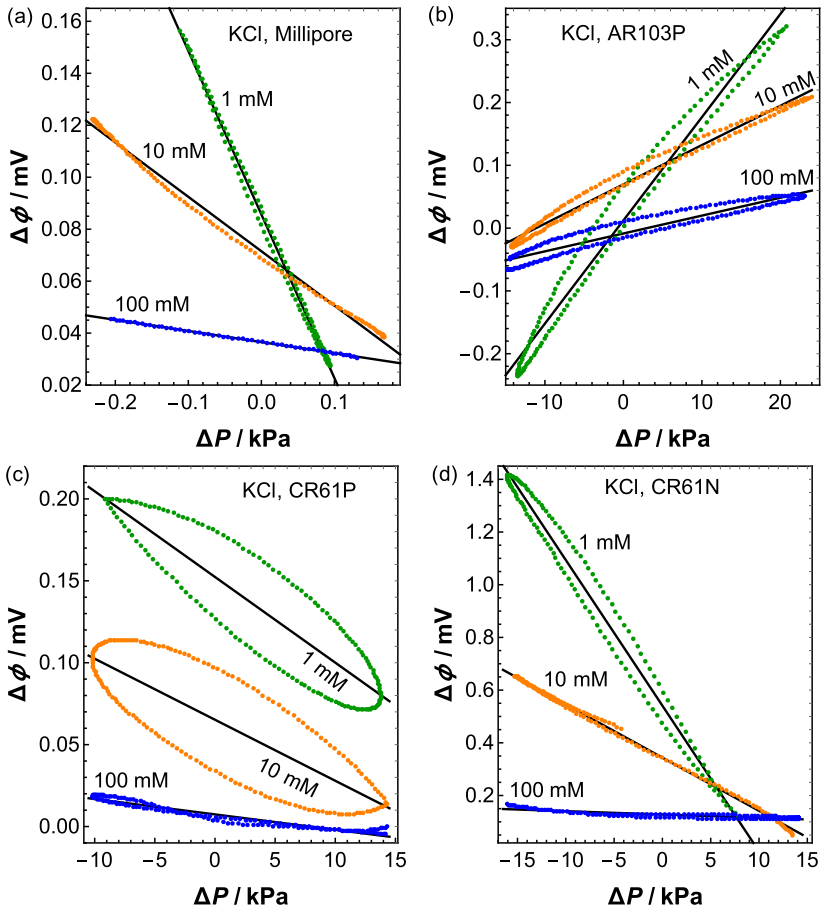

Figure 2. Determination of the streaming potential $\Delta\phi/\Delta P$ of KCl in (a) Millipore VVLP membrane, (b) anion-exchange membrane AR1039, (c) thicker cation-exchange membrane CR61P, and (d) thinner cation-exchange membrane CR61N (vertical offsets have been added for the sake of clarity).

Table 3. Streaming Potential in nV/Pa of the CR61N Membrane with Differing Electrolytes

Cl^- (mM)	KCl	NaCl	$CaCl_2$
1	−55.3 ± 0.6	−9.45 ± 0.06	−16.6 ± 0.2
10	−20.19 ± 0.06	−8.54 ± 0.05	−11.8 ± 0.1
100	−1.26 ± 0.06	−2.68 ± 0.02	−2.91 ± 0.01

measurements at very low electrolyte concentrations are often affected by higher uncertainties. Hence, the correction described by eq 5 was not made to our measurements.

THEORETICAL

An IEM separates two external solutions with the same concentration c^b of the same binary electrolyte. The external solutions are denoted as "left" L, at $x = 0$, and "right" R, at $x =$

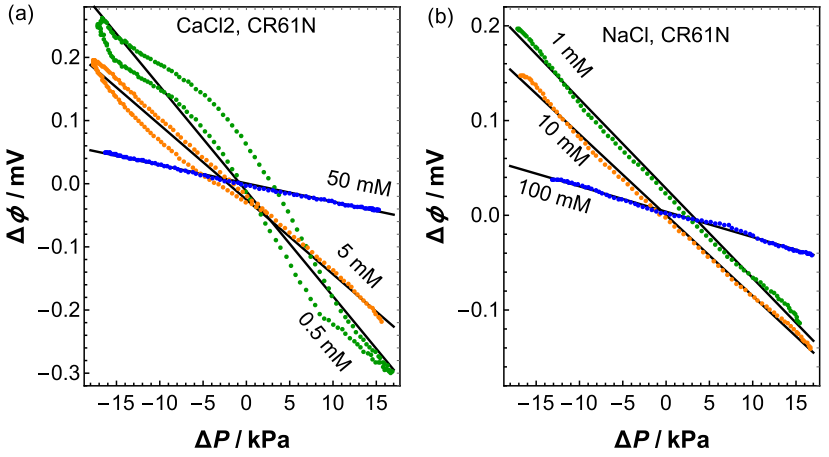

Figure 3. Effect of the counterion on streaming potential of the CR61N membrane: (a) calcium and (b) sodium. Figure 2 shows the KCl measurements.

https://doi.org/10.1021/acs.langmuir.4c00027
Langmuir XXXX, XXX, XXX−XXX

L, where L is the membrane thickness and x is the position coordinate normal to the IEM. The IEM has a concentration $X > 0$ of fixed-charge groups with the same charge number z_2 as the co-ion. When pressure difference $\Delta P = P^L - P^R$ is applied to the external solutions, electric potential difference $\Delta\phi = \phi^L - \phi^R$ can be measured under steady-state, open-circuit conditions. The streaming potential $\nu \equiv (\Delta\phi/\Delta P)_{I=0}$, eq 3, has the same sign as the charge of the fixed groups, i.e., the same sign as z_2. The solution flow induced by ΔP pushes toward the low-pressure external solution an internal solution with an average electric charge density $\langle\rho_e\rangle = -z_2FX$ that compensates for that of the fixed-charge groups. Hence, the sign of $\Delta\phi$ is that of z_2.

Insights on the streaming potential (of homogeneous IEMs and porous membranes) can be obtained by using the capillary SCM.[8−10,19,20,26,35] In this model, the membrane is considered to be an array of parallel cylindrical pores of radius a. The streaming potential can be evaluated from the radial distribution of solution velocity $v(r)$ and electric potential $\psi(r)$ in the radial electrical double layer. The velocity $v(r)$ is obtained by integration of the equation that results from the elimination of the electric charge density ρ_e between the radial Poisson equation and the Navier−Stokes equation.

The electric potential $\psi(r)$ is obtained as the solution of the Poisson−Boltzmann equation (PBE). The Debye screening length inside the membrane is $1/\kappa_D^M \equiv (\epsilon RT)^{1/2}/(z_2F[X^2 + (2c^b)^2]^{1/4})$.[26] The dimensionless pore radius

$$\tilde{a} \equiv \kappa_D^M a \tag{6}$$

determines whether pores are wide or narrow. In narrow pores, $\tilde{a} \ll 1$, there is overlap of the radial electrical double layers, and the pore center is not electroneutral. In wide pores, $\tilde{a} \gg 1$, the pore center is electroneutral. The (dimensionless) Donnan potential $\tilde{\psi}_D$ is defined by the condition $\sinh\tilde{\psi}_D = \langle\sinh\tilde{\psi}\rangle$, where the angle brackets denote the average value across the pore cross-section (see the Appendix). An analytical approximation of $\psi(r)$ can be obtained by assuming that the deviation of the local potential from the Donnan potential is small. This assumption is very accurate when $\tilde{a} < 3$. It is also accurate for $\tilde{a} > 3$ and weakly charged membranes, when the decrease of $\tanh\tilde{\psi}_D = [1 + (2c^b/X)^2]^{(-1/2)}$ with increasing c^b is noticeable. However, it is not accurate for pore radii much larger than the Debye screening length and large surface charge densities at the pore walls. In the latter case, a numerical solution of PBE is necessary.

As shown in the Appendix, the streaming potential for symmetric electrolytes with $\tilde{a} < 3$ is

$$\nu = \nu_\infty \frac{4I_2(\tilde{a})}{\tilde{a}I_1(\tilde{a})}\left[1 + \frac{c_{2D}}{t_1^b X} - 2\nu_\infty\langle\rho_e\rangle\left(1 - \frac{I_0(\tilde{a})I_2(\tilde{a})}{I_1(\tilde{a})^2}\right)\right]^{-1} \tag{7}$$

where

$$\nu_\infty \equiv -\frac{a^2}{8z_1 f\eta D_1} \tag{8}$$

is the streaming potential in very narrow pores, which increases as the squared pore radius a^2. In eqs 7 and 8, $f \equiv F/RT$, η is the dynamic viscosity of the solution, z_1 and D_1 are the charge number and diffusion coefficient of the counterion, $t_1^b = z_1D_1/(z_1D_1 - z_2D_2)$ is the transport number of the counterion in the external solutions, c_{2D} is the co-ion concentration in the membrane as evaluated from the Donnan equilibrium, and $I_n(x)$ is the modified Bessel function of the first kind of order n. It should be noted that $\nu_\infty\langle\rho_e\rangle < 0$ and $1 > I_0(\tilde{a})I_2(\tilde{a})/I_1(\tilde{a})^2$. The coefficient $4I_2(\tilde{a})/\tilde{a}I_1(\tilde{a})$ in eq 7 decreases with increasing pores radius, but the proportionality $\nu_\infty \propto a^2$ still dominates. Hence, the streaming potential increases with the pore radius for both narrow and wide pores, in agreement with the observation that it increases with the increase in the membrane water content.

Finally, note that expressing the dependence of ν on the external electrolyte concentration c^b using c_{2D} in eq 7 is just convenient. When the deviation of the local potential from the Donnan potential is small, the average ionic concentrations and the average electric potential inside the capillaries are approximately the same as given by the Donnan equilibrium (see the Appendix). However, it must be stressed that eq 7 is not based on the Donnan model but only on the SCM.

CONCLUSIONS

It is not simple to explain the observation that the external solution has a significant effect on the streaming potential in an IEM at much lower concentrations than expected from the Donnan equilibrium. The Donnan equilibrium should naturally be written in terms of ionic activities and not concentrations. For 1:1 electrolytes, the co-ion concentration is then

$$c_{2D} = -\frac{X}{2} + \sqrt{\left(\frac{X}{2}\right)^2 + \Gamma(c^b)^2} \tag{9}$$

where $\Gamma = (\gamma_{12}^b)^2/\gamma_1\gamma_2$ is the ratio of the activity coefficients in the aqueous and membrane phases. The estimation of the single ionic activity coefficients in the membrane phase (γ_1 and γ_2) is rather hard and probably not sufficient to fully address the observed behavior. As discussed above, membrane swelling (liquid uptake) or structural heterogeneity are more plausible reasons for the failure of the co-ion exclusion.

The second observation is the rather strong hysteresis of the streaming potential plots: the thicker the membrane, the stronger the hysteresis. Its extent can be reduced by substantial averaging of the pressure−voltage data, but it always remains in the plots depending on how rapidly a measurement is carried out, i.e., on the rate of pumping the solution through the membrane. The more rapidly the pressure drop across the membrane is created, the bigger is the hysteresis. This implies that the system is not in a steady state. Due to the changes in the values of the transport quantities at the membrane−solution interface, concentration polarization is formed on both sides of the membrane, which contributes to hysteresis. In the Appendix, a brief description of the formation of the concentration polarization is given.

The observation that streaming potential depends on the membrane thickness cannot be explained with the charged-capillary model as the total pressure and potential drops across the membrane cancel the membrane thickness from the equations. The only plausible explanation is that ions and the solvent pass via different pathways through the membrane, which is rather obvious as the ions can hop from a charged group to another, while the solvent has to use tortuous pathways within the membrane matrix. Taking into account

https://doi.org/10.1021/acs.langmuir.4c00027
Langmuir XXXX, XXX, XXX−XXX

that the modification with S-PEEK is rather straightforward and that Daramic is quite inexpensive compared to commercial IEMs, this membrane provides a competitive alternative in membrane processes.

■ ASSOCIATED CONTENT

Supporting Information

The Supporting Information is available free of charge at https://pubs.acs.org/doi/10.1021/acs.langmuir.4c00027.

Theoretical calculations of the streaming potential using the capillary SCM and effect of concentration polarization (PDF)

■ AUTHOR INFORMATION

Corresponding Author

Lasse Murtomäki − *Department of Chemistry and Materials Science, School of Chemical Engineering, Aalto University, Aalto 00076, Finland;* orcid.org/0000-0001-7667-4325; Phone: +358 505706352; Email: lasse.murtomaki@aalto.fi

Authors

Wouter Badenhorst − *Department of Chemistry and Materials Science, School of Chemical Engineering, Aalto University, Aalto 00076, Finland;* orcid.org/0000-0003-4854-6865

Kuldeep − *Department of Chemistry and Materials Science, School of Chemical Engineering, Aalto University, Aalto 00076, Finland*

Jose Antonio Manzanares − *Department of Thermodynamics, University of Valencia, Burjassot E-46100, Spain;* orcid.org/0000-0002-5402-6842

Complete contact information is available at: https://pubs.acs.org/10.1021/acs.langmuir.4c00027

Author Contributions

Conceptualization: W.B. and L.M.; data curation: W.B. and K.; formal analysis: W.B., K., J.M., and L.M.; funding acquisition: W.B. and L.M.; investigation: W.B. and K.; methodology: W.B.; project administration: W.B. and L.M.; resources: W.B.; software: W.B.; supervision: L.M.; validation: W.B., K., J.M., and L.M.; visualization: K.; writing−original draft: W.B., K., J.M., and L.M.; and writing—review and editing: W.B., K., J.M., and L.M. W.B. and K. contributed equally to this paper.

Notes

The authors declare no competing financial interest.

■ ACKNOWLEDGMENTS

Kuldeep acknowledges grant #210026 from Vilho, Yrjö, and Kalle Vaisala Foundation. Wouter Badenhorst acknowledges the CuBER project, EU Horizon 2020 Programme (H2020/2014-2020), grant agreement #875605. J.A.M. acknowledges the support from the Ministerio de Ciencia e Innovación and European Regional Development Funds (project PID2022-139953NB-I00) and from the Direcció General Ciència i Investigació of the Generalitat Valenciana (project CIAICO/2022/247).

■ REFERENCES

(1) Buonomenna, M. G. Membrane processes for a sustainable industrial growth. *RSC Adv.* **2013**, *3*, 5694−5740.

(2) Kuldeep; Kauranen, P.; Pajari, H.; Pajarre, R.; Murtomäki, L. Electrodiffusion of ions in ion exchange membranes: Finite element simulations and experiments. *Chem. Eng. J. Adv.* **2021**, *8*, 100169.

(3) Kuldeep; Badenhorst, W. D.; Kauranen, P.; Pajari, H.; Ruismäki, R.; Mannela, P.; Murtomäki, L. Bipolar membrane electrodialysis for sulfate recycling in the metallurgical industries. *Membranes* **2021**, *11*, 718.

(4) Kim, D. H. A review of desalting process techniques and economic analysis of the recovery of salts from retentates. *Desalination* **2011**, *270*, 1−8.

(5) Somovilla, P.; Villaluenga, J.; Barragán, V.; Izquierdo-Gil, M. Experimental determination of the streaming potential across cation-exchange membranes with different morphologies. *J. Membr. Sci.* **2016**, *500*, 16−24.

(6) Barragán, V.; Villaluenga, J.; Izquierdo-Gil, M. A.; Kristiansen, K. On the electrokinetic characterization of charged polymeric membranes by transversal streaming potential. *Electrochim. Acta* **2021**, *387*, 138462.

(7) Aguilella, V.; Kontturi, K.; Murtomäki, L.; Ramírez, P. Estimation of the pore size and charge density in human cadaver skin. *J. Controlled Release* **1994**, *32*, 249−257.

(8) Mafé, S.; Manzanares, J.; Pellicer, J. On the introduction of the pore wall charge in the space-charge model for microporous membranes. *J. Membr. Sci.* **1990**, *51*, 161−168.

(9) Manzanares, J. A.; Mafé, S.; Ramírez, P. Pore conductivity and streaming potential in charged capillary tubes with concentration dependent pore wall charge. *J. Non-Equilib. Thermodyn.* **1991**, *16*, 255−265.

(10) Kontturi, K.; Savonen, A.; Vuoristo, M.; Volden, H. V.; Wang, D.-N.; Paulsen, G. B.; Nielsen, R. I.; Olsen, C. E.; Pedersen, C.; Stidsen, C. E. Study of adsorption and ion-exchange properties of some porous membranes. *Acta Chem. Scand.* **1994**, *48*, 1−11.

(11) Raiman, J.; Hänninen, K.; Kontturi, K.; Murtomäki, L.; Hirvonen, J. Drug adsorption in human skin: a streaming potential study. *J. Pharm. Sci.* **2003**, *92*, 2366−2372.

(12) Murtomäki, L.; Vainikka, T.; Pescina, S.; Nicoli, S. Drug adsorption on bovine and porcine sclera studied with streaming potential. *J. Pharm. Sci.* **2013**, *102*, 2264−2272.

(13) Caplan, S. R.; Mikulecky, D. C. *Ion Exchange*; Marinsky, J. A., Ed.; Marcel Dekker, 1966; Chapter 1, pp 1−64.

(14) Rastogi, R.; Srivastava, R.; Singh, S. Nonequilibrium thermodynamics of electrokinetic phenomena. *Chem. Rev.* **1993**, *93*, 1945−1990.

(15) Lakshminarayanaiah, N. *Transport Phenomena in Membranes*; Academic Press, 1969; p 267.

(16) Brun, T.; Vaula, D. Correlation of measurements of electroosmosis and streaming potentials in ion exchanger membranes. *Ber. Bunsenges. Phys. Chem.* **1967**, *71*, 824−829.

(17) Trivijitkasem, P.; Østvold, T. Water transport in ion exchange membranes. *Electrochim. Acta* **1980**, *25*, 171−178.

(18) Sørensen, T. S.; Koefoed, J. Electrokinetic effects in charged capillary tubes. *J. Chem. Soc., Faraday Trans. 2* **1974**, *70*, 665−675.

(19) Cervera, J.; Manzanares, J. A.; Mafé, S. Ion size effects on the streaming potential of narrow charged pores. *Phys. Chem. Chem. Phys.* **2001**, *3*, 2493−2496.

(20) Westermann-Clark, G.; Anderson, J. Experimental verification of the space-charge model for electrokinetics in charged microporous membranes. *J. Electrochem. Soc.* **1983**, *130*, 839−847.

(21) Katchalsky, A.; Curran, P. F. *Nonequilibrium Thermodynamics in Biophysics*; Harvard University Press, 1965; p 172.

(22) Reynard, J. M.; Larchet, C.; Bulvestre, G.; Auclair, B. Determination of the streaming potential in ion-exchange membranes. *J. Membr. Sci.* **1992**, *67*, 57−66.

(23) Toyoshima, Y.; Nozaki, H. Streaming potential across a charged membrane. *J. Phys. Chem.* **1969**, *73*, 2134−2141.

(24) Tasaka, M.; Tamura, S.; Takemura, N.; Morimoto, K. Concentration dependence of electroosmosis and streaming potential across charged membranes. *J. Membr. Sci.* **1982**, *12*, 169−182.

(25) Zhang, Y.; Xu, T. An experimental investigation of streaming potentials through homogeneous ion-exchange membranes. *Desalination* **2006**, *190*, 256−266.
(26) Kontturi, K. K.; Murtomäki, L.; Manzanares, J. A. *Ionic Transport Processes: in Electrochemistry and Membrane Science*; Oxford University Press, 2015; pp 163−167 ff and 205 ff.
(27) Manzanares, J. A.; Mafe, S.; Pellicer, J. Current efficiency enhancement in membranes with macroscopic inhomogeneities in the fixed charge distribution. *J. Chem. Soc., Faraday Trans.* **1992**, *88*, 2355−2364.
(28) Sokirko, A. V.; Manzanares, J. A.; Pellicer, J. The permselectivity of membrane systems with an inhomogeneous distribution of fixed charge groups. *J. Colloid Interface Sci.* **1994**, *168*, 32−39.
(29) Huisman, I. H.; Pradanos, P.; Hernández, A. Electrokinetic characterisation of ultrafiltration membranes by streaming potential, electroviscous effect, and salt retention. *J. Membr. Sci.* **2000**, *178*, 55−64.
(30) Calvo, J.; Hernández, A.; Prádanos, P.; Tejerina, F. Charge adsorption and zeta potential in cyclopore membranes. *J. Colloid Interface Sci.* **1996**, *181*, 399−412.
(31) Xi, J.; Li, Z.; Yu, L.; Yin, B.; Wang, L.; Liu, L.; Qiu, X.; Chen, L. Effect of degree of sulfonation and casting solvent on sulfonated poly (ether ether ketone) membrane for vanadium redox flow battery. *J. Power Sources* **2015**, *285*, 195−204.
(32) Yuan, J.; Pan, Z.-Z.; Jin, Y.; Qiu, Q.; Zhang, C.; Zhao, Y.; Li, Y. Membranes in non-aqueous redox flow battery: A review. *J. Power Sources* **2021**, *500*, 229983.
(33) Izquierdo-Gil, M. A.; Barragán, V.; Villaluenga, J.; Godino, M. Water uptake and salt transport through Nafion cation-exchange membranes with different thicknesses. *Chem. Eng. Sci.* **2012**, *72*, 1−9.
(34) Kuldeep; Manzanares, J. A.; Kauranen, P.; Mousavihashemi, S.; Murtomäki, L. Determination of ionic diffusion coefficients in ion-exchange membranes: Strong electrolytes and sulfates with dissociation equilibria. *ChemElectroChem.* **2022**, *9*, No. e202200403.
(35) Cervera, J.; García-Morales, V.; Pellicer, J. Ion size effects on the electrokinetic flow in nanoporous membranes caused by concentration gradients. *J. Phys. Chem. B* **2003**, *107*, 8300−8309.
(36) Spiegler, K. On the measurement of streaming potentials with silver-silver chloride electrodes. *Desalination* **1974**, *15*, 135−140.

https://doi.org/10.1021/acs.langmuir.4c00027
Langmuir XXXX, XXX, XXX−XXX

Supporting Information
Unexpected behaviour of streaming potential in ion-exchange membranes

Wouter Badenhorst,[†,¶] Kuldeep,[†,¶] Jose Antonio Manzanares,[‡] and Lasse Murtomäki[*,]

[†]*Department of Chemistry and Materials Science, School of Chemical Engineering, Aalto University PO Box 1600, 00076 AALTO, Finland*

[‡]*Department of Thermodynamics, University of Valencia, c/Dr. Moliner, 50. E-46100 Burjassot, Spain*

[¶]*W.B. and K. contributed equally to this paper.*

E-mail: lasse.murtomaki@aalto.fi

Phone: +358 505706352

Appendix

Theory of streaming potential in membranes based on the capillary space-charge model

An ion-exchange membrane (IEM) separates two external solutions with the same concentration c^b of the same binary electrolyte. The external solutions are denoted as "left" L, at $x = 0$, and "right" R, at $x = L$, where L is the membrane thickness and x is the position coordinate normal to the IEM. The IEM has a concentration $X > 0$ of fixed charge groups

with the same charge number z_2 as the co-ion.

When a pressure difference $\Delta P = P^{\mathrm{L}} - P^{\mathrm{R}}$ is applied to the external solutions, an electric potential difference $\Delta\phi = \phi^{\mathrm{L}} - \phi^{\mathrm{R}}$ can be measured under steady-state, open-circuit conditions. The streaming potential $\nu \equiv (\Delta\phi/\Delta P)_{I=0}$ (Eq. 3 in the main text) has the same sign as the charge of the fixed groups. The solution flow induced by ΔP pushes, towards the low-pressure external solution, an internal solution with an average electric charge density

$$\langle \rho_{\mathrm{e}} \rangle \equiv F \left(z_1 \langle c_1 \rangle + z_2 \langle c_2 \rangle \right) = -z_2 F X \tag{1}$$

that compensates for that of the fixed charge groups; subscripts 1 and 2 denote the counterion and co-ion, respectively. Hence, the sign of the electric potential difference between the high- and low-pressure solutions is that of z_2. In Eq. 1, c_i ($i = 1, 2$) are the ionic molar concentrations and the angle brackets denote the average value inside the IEM.

The phenomenological transport equations (Eqs. 1 and 2 in the main text) relate ΔP and $\Delta\phi$ to the solution volume flow $J_V = A\langle v \rangle$ and the electric current $I = A\langle i \rangle$, where $\langle v \rangle$ is the average solution velocity, $\langle i \rangle$ is the average electric current density, and A is the membrane area. In streaming potential (SP) measurements, the flux density j_i of ionic species i across the IEM has conductive and convective but no diffusive contribution,[1]

$$j_i = -z_i D_i c_i \frac{\mathrm{d}V}{\mathrm{d}x} - \frac{D_i c_i}{RT} \left(V_i - \frac{M_i}{M_{\mathrm{s}}} V_{\mathrm{s}} \right) \left(\frac{\partial P}{\partial x} \right)_r + c_i v \,, \tag{2}$$

where D_i is its diffusion coefficient, $\mathrm{d}V/\mathrm{d}x = -\Delta\phi/L$ is the axial electric field, V_i and V_{s} are the molar partial volumes of ionic species i and the solvent, M_i and M_{s} are the molar masses of ionic species i and the solvent, and v is the solution velocity. Most often, the pressure gradient contribution to j_i in Eq. 2 is neglected,[2,3] which is justified when the solutions are not very concentrated and the ion size effects are minor.[1,4] Then, the average value of the

current density $i = F\left(z_1 j_1 + z_2 j_2\right)$ reduces to

$$\langle i \rangle \approx \langle \sigma \rangle \frac{\Delta\phi}{L} + \langle \rho_{\mathrm{e}} v \rangle \ . \tag{3}$$

In Eq. 3, the average electrical conductivity of the membrane solution is

$$\langle \sigma \rangle = \frac{F^2}{RT}\left(z_1^2 D_1 \langle c_1 \rangle + z_2^2 D_2 \langle c_2 \rangle\right) = \sigma_\infty \left(1 + \frac{\langle c_2 \rangle}{t_1^{\mathrm{b}} X}\right) , \tag{4}$$

where $\sigma_\infty \equiv f z_1 D_1 \langle \rho_{\mathrm{e}} \rangle > 0$, $f \equiv F/RT$, $t_1^{\mathrm{b}} = z_1 D_1 / \left(z_1 D_1 - z_2 D_2\right)$ is the transport number of the counterion in the external solutions, and we have used Eq. 1, $z_1 \langle c_1 \rangle = \langle \rho_{\mathrm{e}} \rangle / F - z_2 \langle c_2 \rangle$. The average co-ion concentration $\langle c_2 \rangle$, and hence $\langle \sigma \rangle$, decreases with decreasing c^{b}. Its lowest value is $\langle \sigma \rangle \approx \sigma_\infty$ when $c^{\mathrm{b}} \ll X$, i.e., in strongly-charged IEMs.

In the capillary space-charge model (SCM) the membrane is considered to be an array of parallel cylindrical pores of radius a.[1,3–8] The average value of any function $\varphi(r)$ of the radial coordinate is then given by $\langle \varphi \rangle \pi a^2 \equiv \int_0^a \varphi(r) 2\pi r \, \mathrm{d}r$. The surface density of electric charge at the pore walls is σ_{M} and its volume equivalent is $z_2 F X = 2\sigma_{\mathrm{M}}/a$. This fixed charge is compensated by that of the ions in the membrane pores, Eq. 1. In SP measurements, the electric potential is conveniently decomposed into two contributions, $\phi(x, r) = V(x) + \psi(r)$, where $\psi(r)$ is the solution of the (radial) Poisson equation

$$\frac{\epsilon}{r}\frac{\mathrm{d}}{\mathrm{d}r}\left(r\frac{\mathrm{d}\psi}{\mathrm{d}r}\right) = -\rho_{\mathrm{e}}(r) \tag{5}$$

and ϵ is the electrical permittivity of the electrolyte solution. The solution velocity v is obtained by solving the Navier-Stokes equation

$$\frac{\eta}{r}\frac{\mathrm{d}}{\mathrm{d}r}\left(r\frac{\mathrm{d}v}{\mathrm{d}r}\right) = \left(\frac{\partial P}{\partial x}\right)_r + \rho_{\mathrm{e}}\frac{\mathrm{d}V}{\mathrm{d}x} , \tag{6}$$

where $(\partial P/\partial x)_r = -\Delta P/L$ and $\mathrm{d}V/\mathrm{d}x = -\Delta\phi/L$. The electric potential difference between

the external solutions is $\Delta\phi = \Delta V$ because they have the same electrolyte and concentration.

Elimination of the electric charge density ρ_e between Eqs. 5 and 6, followed by integration using the boundary conditions at the pore axis, $\mathrm{d}v/\,\mathrm{d}r|_{r=0} = 0$ and $\mathrm{d}\psi/\,\mathrm{d}r|_{r=0} = 0$, leads to

$$\eta \frac{\mathrm{d}v}{\mathrm{d}r} = \frac{r}{2}\left(\frac{\partial P}{\partial x}\right)_r - \epsilon \frac{\mathrm{d}\psi}{\mathrm{d}r}\frac{\mathrm{d}V}{\mathrm{d}x}\,. \tag{7}$$

Its integration gives the radial distribution of the velocity

$$v(r) = \frac{a^2 - r^2}{4\eta L}\Delta P - \frac{\epsilon}{\eta L}[\psi(a) - \psi(r)]\Delta\phi\,. \tag{8}$$

As required by thermodynamic stability, ΔP generates a volume flow that, in turn, generates a $\Delta\phi$ that tends to reduce the volume flow; note that $\Delta\phi/\Delta P$ and $\psi(a) - \psi(r)$ have both the same sign as the fixed charge. The superposition principle applied to Eq. 6 implies that v can be written as $v(r) = v_{\Delta P}(r) + v_{\Delta\phi}(r)$, with $v_{\Delta P}$ proportional to ΔP and $v_{\Delta\phi}$ proportional to $\Delta\phi$; see Eq. 8. The pore average value of the first contribution is $\langle v_{\Delta P}\rangle = (a^2/8\eta)\,\Delta P/L$.

The Onsager reciprocal relation $L_{21} = L_{12}$ immediately follows from Eq. 8. We note that Eqs. 1 and 2 in the main text and Eq. 3 imply $A\,\langle v_{\Delta\phi}\rangle = L_{12}\Delta\phi$ and $A\,\langle \rho_e v_{\Delta P}\rangle = L_{21}\Delta P$. Thus, Eq. 6 implies $L_{21} = L_{12}$ because

$$\begin{aligned}\langle \rho_e v_{\Delta P}\rangle \frac{\mathrm{d}V}{\mathrm{d}x} &= \eta\left\langle \frac{v_{\Delta P}}{r}\frac{\mathrm{d}}{\mathrm{d}r}\left(r\frac{\mathrm{d}v_{\Delta\phi}}{\mathrm{d}r}\right)\right\rangle \\ &= \eta\left\langle \frac{v_{\Delta\phi}}{r}\frac{\mathrm{d}}{\mathrm{d}r}\left(r\frac{\mathrm{d}v_{\Delta P}}{\mathrm{d}r}\right)\right\rangle = \langle v_{\Delta\phi}\rangle\left(\frac{\partial P}{\partial x}\right)_r\,,\end{aligned} \tag{9}$$

where we have used the non-slip condition $v_{\Delta P}(a) = v_{\Delta\phi}(a) = v(a) = 0$ at the pore wall.

The streaming potential is determined by the radial distribution of the electric potential inside the membrane pores. Equation 8 implies $\langle v_{\Delta\phi}\rangle\, L/\Delta\phi = -(\epsilon/\eta)[\psi(a) - \langle\psi\rangle]$. Substi-

tution of $v = v_{\Delta P} + v_{\Delta\phi}$ in Eq. 3 allows us to express the streaming potential as

$$\nu \equiv \left(\frac{\Delta\phi}{\Delta P}\right)_{\langle i\rangle=0} = -\frac{\langle \rho_{\rm e} v_{\Delta P}\rangle\, L/\Delta P}{\langle\sigma\rangle + \langle \rho_{\rm e} v_{\Delta\phi}\rangle\, L/\Delta\phi} = -\frac{\langle v_{\Delta\phi}\rangle\, L/\Delta\phi}{\langle\sigma\rangle_{\rm eff}} = \frac{\epsilon}{\eta}\frac{\psi(a) - \langle\psi\rangle}{\langle\sigma\rangle_{\rm eff}}\,, \tag{10}$$

where $\langle\sigma\rangle_{\rm eff} \equiv \langle\sigma\rangle + \langle\rho_{\rm e}\nu_{\Delta\phi}\rangle\, L/\Delta\phi$ is the effective conductivity and we have used Eq. 8. Note that $\psi(a) - \langle\psi\rangle$ has the same sign as the charge of the fixed groups, in agreement with the above explanation on the sign of ν. For narrow pores, which correspond to low membrane water content, $|\psi(a) - \langle\psi\rangle|$ and $|\nu|$ are small. For wide pores, which correspond to high membrane water content, $|\psi(a) - \langle\psi\rangle|$ and $|\nu|$ are large, as observed experimentally.

To evaluate the streaming potential from Eq. 10, we need the electric potential $\psi(r)$ in the radial electrical double layer, which is the solution of the Poisson-Boltzmann equation (PBE). For symmetric electrolytes, the ionic concentrations are $c_1(r) = c^{\rm b}{\rm e}^{\tilde{\psi}}$ and $c_2(r) = c^{\rm b}{\rm e}^{-\tilde{\psi}}$, where $\tilde{\psi}(r) \equiv z_2 f\psi(r) > 0$. The electrical charge density in the cylindrical pore is $\rho_{\rm e}(r) = -2z_2 F c^{\rm b}\sinh\tilde{\psi}$. The global electroneutrality, Eq. 1, requires

$$\langle\sinh\tilde{\psi}\rangle = -\frac{\langle\rho_{\rm e}\rangle}{2z_2 F c^{\rm b}} = \frac{X}{2c^{\rm b}} \equiv \sinh\tilde{\psi}_{\rm D}\,, \tag{11}$$

which defines the (dimensionless) Donnan potential $\tilde{\psi}_{\rm D} > 0$. When the deviation of the potential $\tilde{\psi}$ from the Donnan value $\tilde{\psi}_{\rm D}$ is small, $\left|\tilde{\psi}(r) - \tilde{\psi}_{\rm D}\right| \ll 1$, we can use the approximation

$$\sinh\tilde{\psi} \approx \sinh\tilde{\psi}_{\rm D} + \cosh\tilde{\psi}_{\rm D}\left[\tilde{\psi} - \tilde{\psi}_{\rm D}\right] \equiv \varphi(r)\cosh\tilde{\psi}_{\rm D}\,, \tag{12}$$

where

$$\varphi(r) \equiv \tilde{\psi}(r) - \tilde{\psi}_{\rm D} + \tanh\tilde{\psi}_{\rm D}\,. \tag{13}$$

The electrostatic interactions are screened inside the radial electrical double layer. A very good estimation for the screening length is the reciprocal of the Debye parameter $\kappa_{\rm D}^{\rm M}$,

defined as

$$\left(\kappa_{\rm D}^{\rm M}\right)^2 \equiv \frac{z_2^2 F^2 \left(c_{1\rm D} + c_{2\rm D}\right)}{\epsilon RT} = \frac{-z_2 f \left\langle \rho_{\rm e} \right\rangle}{\epsilon \tanh \widetilde{\psi}_{\rm D}} > 0 \,, \tag{14}$$

where $c_{1\rm D} \equiv c^{\rm b} {\rm e}^{\widetilde{\psi}_{\rm D}}$ and $c_{2\rm D} \equiv c^{\rm b} {\rm e}^{-\widetilde{\psi}_{\rm D}}$ are the ionic concentrations as evaluated from the Donnan equilibrium, and $c_{1\rm D} + c_{2\rm D} = 2c^{\rm b} \cosh \tilde{\psi}_{\rm D} = [X^2 + (2c^{\rm b})^2]^{1/2}$. With Eq. 12, the electric charge density becomes $\rho_{\rm e} \approx -(2z_2 F c^{\rm b} \cosh \tilde{\psi}_{\rm D})\varphi = -(\epsilon / z_2 f) \left(\kappa_{\rm D}^{\rm M}\right)^2 \varphi$, and substitution in Eq. 5 gives the linearized PBE

$$\frac{1}{r} \frac{\rm d}{{\rm d}r} \left(r \frac{{\rm d}\varphi}{{\rm d}r} \right) \approx \left(\kappa_{\rm D}^{\rm M}\right)^2 \varphi \,, \tag{15}$$

which is subject to the boundary condition

$$\left. \frac{{\rm d}\varphi}{{\rm d}r} \right|_{r=a} = z_2 f \frac{\sigma_{\rm M}}{\epsilon} = \frac{a}{2} \left(\kappa_{\rm D}^{\rm M}\right)^2 \tanh \tilde{\psi}_{\rm D} \,, \tag{16}$$

where $\sigma_{\rm M} = z_2 F X a/2$ is the surface density of electric charge at the pore walls. The solution of Eqs. 15 and 16 is[8]

$$\tilde{\psi}(r) \approx \tilde{\psi}_{\rm D} + \left[\frac{\kappa_{\rm D}^{\rm M} a}{2} \frac{I_0(\kappa_{\rm D}^{\rm M} r)}{I_1(\kappa_{\rm D}^{\rm M} a)} - 1 \right] \tanh \tilde{\psi}_{\rm D} \,, \tag{17}$$

where $I_n(x)$ is the modified Bessel function of the first kind of order n. Note that Eq. 17 implies that $\langle \tilde{\psi} \rangle \approx \tilde{\psi}_{\rm D}$ and, hence, that the average ionic concentrations are $\langle c_1 \rangle \approx c_{1\rm D}$ and $\langle c_2 \rangle \approx c_{2\rm D}$.

The dimensionless pore radius

$$\tilde{a} \equiv \kappa_{\rm D}^{\rm M} a \tag{18}$$

determines whether pores are wide or narrow. For instance, narrow pores mean that the pore radius is smaller than the Debye screening length $1/\kappa_{\rm D}^{\rm M}$. The electrical charge density at the pore centre is $\rho_{\rm e}(0) = -(2z_2 F c^{\rm b} \cosh \tilde{\psi}_{\rm D})\varphi(0) = \langle \rho_{\rm e} \rangle \, \tilde{a}/2I_1(\tilde{a})$. At the centre of very narrow pores, $\rho_{\rm e}(0) \approx \langle \rho_{\rm e} \rangle = -z_2 F X$ if $\tilde{a} \ll 1$. The centre of wide pores is practically

electroneutral, $\rho_{\rm e}(0) \approx 0$ if $\tilde{a} \gg 1$. Note that the PBE has been solved under the assumption $\left|\tilde{\psi}(a) - \tilde{\psi}_{\rm D}\right| \ll 1$. If $X/c^{\rm b}$ is so large that $\tanh\tilde{\psi}_{\rm D} \approx 1$ then Eq. 17 should not be used when $\tilde{a} > 3$. Equation 17 may remain valid for $\tilde{a} > 3$ when the decrease of $\tanh\tilde{\psi}_{\rm D} = [1 + (2c^{\rm b}/X)^2]^{-1/2}$ with increasing $c^{\rm b}$ is noticeable. From Eq. 17 we can evaluate

$$\begin{aligned}\tilde{\psi}(a) - \langle\tilde{\psi}\rangle &\approx \frac{z_2 f\sigma_{\rm M} a}{\epsilon}\frac{I_0(\tilde{a}) - \left\langle I_0(\kappa_{\rm D}^{\rm M} r)\right\rangle}{\tilde{a} I_1(\tilde{a})} \\ &= \frac{z_2 f\sigma_{\rm M}}{\kappa_{\rm D}^{\rm M}\epsilon}\left[\frac{I_0(\tilde{a})}{I_1(\tilde{a})} - \frac{2}{\tilde{a}}\right] = \tanh\tilde{\psi}_{\rm D}\frac{\tilde{a}\, I_2(\tilde{a})}{2I_1(\tilde{a})}\,, \end{aligned} \tag{19}$$

where we have used $I_2(\tilde{a}) = I_0(\tilde{a}) - 2I_1(\tilde{a})/\tilde{a}$ and $z_2 f\sigma_{\rm M}/\kappa_{\rm D}^{\rm M}\epsilon = (\tilde{a}/2)\tanh\tilde{\psi}_{\rm D}$. For narrow pores, $[\tilde{\psi}(a) - \langle\tilde{\psi}\rangle]_{\tilde{a}\ll 1} \approx (\tilde{a}^2/8)\tanh\tilde{\psi}_{\rm D}$ is small. Then, the reference value of the streaming potential for narrow pores is

$$\nu_\infty \equiv \frac{\epsilon}{\eta\sigma_\infty}[\psi(a) - \langle\psi\rangle]_{\tilde{a}\ll 1} \approx -\frac{a^2}{8z_1 f\eta D_1}\,, \tag{20}$$

where we have used $z_1 = -z_2$, $\sigma_\infty \equiv f z_1 D_1 \langle\rho_{\rm e}\rangle$, and Eqs. 10 and 14. For wide pores, $[\tilde{\psi}(a) - \langle\tilde{\psi}\rangle]_{\tilde{a}\gg 1}$ increases almost linearly with $\tilde{a}$, but a numerical solution of the PBE is required when $\left|\tilde{\psi}(a) - \tilde{\psi}_{\rm D}\right| > 1$.

The streaming potential, Eq. 10, can be now evaluated. From Eq. 17 we have

$$\frac{\langle\rho_{\rm e} v_{\Delta\phi}\rangle}{\sigma_\infty \Delta\phi/L} = \frac{2\epsilon RTc^{\rm b}}{\sigma_\infty\eta}\langle[\tilde{\psi}(a) - \tilde{\psi}(r)]\sinh\tilde{\psi}(r)\rangle \approx -2\nu_\infty\langle\rho_{\rm e}\rangle\left[1 - \frac{I_0(\tilde{a})I_2(\tilde{a})}{I_1(\tilde{a})^2}\right] \tag{21}$$

and then, with the conductivity in Eq. 4, we obtain

$$\begin{aligned}\nu &= \frac{\epsilon}{z_2 f\eta}\frac{\tilde{\psi}(a) - \langle\tilde{\psi}\rangle}{\langle\sigma\rangle_{\rm eff}} = \frac{\epsilon[\tilde{\psi}(a) - \langle\tilde{\psi}\rangle]}{z_2 f\eta\sigma_\infty}\left[\frac{\langle\sigma\rangle}{\sigma_\infty} + \frac{\langle\rho_{\rm e} v_{\Delta\phi}\rangle}{\sigma_\infty\Delta\phi/L}\right]^{-1} \\ &= \nu_\infty\frac{4I_2(\tilde{a})}{\tilde{a} I_1(\tilde{a})}\left[1 + \frac{c_{\rm 2D}}{t_1^{\rm b} X} - 2\nu_\infty\langle\rho_{\rm e}\rangle\left(1 - \frac{I_0(\tilde{a})I_2(\tilde{a})}{I_1(\tilde{a})^2}\right)\right]^{-1}\,, \end{aligned} \tag{22}$$

where it should be noted that $\nu_\infty\langle\rho_{\rm e}\rangle < 0$ and $1 > I_0(\tilde{a})I_2(\tilde{a})/I_1(\tilde{a})^2$. Equation 22 agrees qualitatively with the experimental observations (Fig. 1). It is noticeable, as it has been

evidenced since the early theoretical studies on the streaming potential,[9] that the effective fixed-charge concentration that describes the observed dependence of the streaming potential with the electrolyte concentration (Table 2, main text) is significantly smaller than the actual concentration of fixed-charge groups. For narrow pores, the streaming potential is

$$\nu \approx \nu_\infty \left[1 + \frac{c_{2D}}{t_1^b X} - \nu_\infty \langle \rho_e \rangle \right]^{-1} \quad (\tilde{a} \ll 1) \,, \tag{23}$$

which increases as the squared pore radius. The coefficient $4I_2(\tilde{a})/\tilde{a}I_1(\tilde{a})$ in Eq. 22 decreases with increasing the pores radius, but the proportionality $\nu_\infty \propto a^2$ still dominates. Thence, the streaming potential increases with the pore radius for both narrow and wide pores, in agreement with the observation that it increases with the increase in the membrane water content.

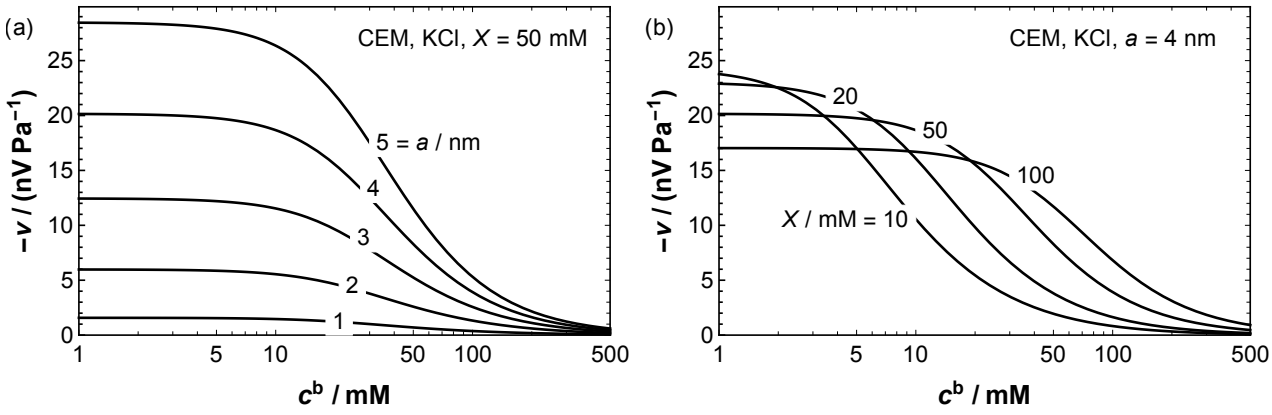

Figure 1: The streaming potential decreases with increasing electrolyte concentration and increases with increasing pore radius. For narrow pores, its limiting value ν_∞ at very low electrolyte concentrations is independent of the effective fixed charge density X. (b) For wide pores, the limiting value of the streaming potential increases with decreasing effective fixed charge density X; should a pore radius $a = 1$ nm be considered in panel (b) then the dependence of ν_∞ on X would be practically insignificant.

Remarks on concentration polarization during streaming potential measurements

In streaming potential measurements, the membrane separates two identical electrolyte solutions with the same concentration. The applied pressure difference generates a solution flow and, therefore, a flow of electrolyte. Due to co-ion exclusion, the IEMs have a low electrolyte permeability. Concentration polarization develops because the electrolyte accumulates in the high-pressure, external membrane surface and depletes in the low-pressure external membrane surface. Since the electrolyte flux density is small, we can consider first a simple model with total co-ion exclusion and no electrolyte flux density. The pressure decreases in the direction of increasing x and the solution velocity $v = -k\ \mathrm{d}P/\mathrm{d}x$ is positive, where k is a proportionality constant related to the hydraulic permeability, e.g., $k = a^2/8\eta$ in the Poiseuille flow across capillaries of radius a. In the membrane, the equation for the counterion flux density is

$$j_1 = 0 = -z_1 D_1 c_1 f \frac{\mathrm{d}V}{\mathrm{d}x} + c_1 v \tag{24}$$

and the streaming potential is

$$\nu = \frac{\mathrm{d}V/\mathrm{d}x}{\mathrm{d}P/\mathrm{d}x} = \frac{v/z_1 f D_1}{-v/k} = -\frac{k}{z_1 f D_1}\,. \tag{25}$$

The solution velocity in the membrane pores is larger than in the diffusion boundary layers (DBLs) in a factor $1/\varepsilon$, where ε is the membrane porosity. In the DBLs of thickness δ, the equation for the electrolyte flux density is

$$\varepsilon j_\pm = 0 = -D_{12}\frac{\mathrm{d}c}{\mathrm{d}x} + c\varepsilon v \rightarrow \mathrm{d}\ln c = (\mathrm{Pe}/\delta)\mathrm{d}x \tag{26}$$

$$c(x) = c^{\mathrm{b}} \exp[(x+\delta)\mathrm{Pe}/\delta] \geq c^{\mathrm{b}}, \quad -\delta \leq x \leq 0 \tag{27}$$

$$c(x) = c^{\mathrm{b}} \exp[-(L+\delta-x)\mathrm{Pe}/\delta] \leq c^{\mathrm{b}}, \quad L \leq x \leq L+\delta\,, \tag{28}$$

where $\mathrm{Pe} = \varepsilon v\delta/D_{12} \geq 0$ is the Peclet number (in the DBLs), D_{12} is the electrolyte diffusion coefficient, i.e., $D_{12} = 2D_1D_2/(D_1 + D_2)$ for symmetric electrolytes. The conclusion from Eqs. 27 and 28 is that the concentrations at the external membrane boundaries are different, $c(0) = c^{\mathrm{b}}\mathrm{e}^{\mathrm{Pe}}$ and $c(L) = c^{\mathrm{b}}\mathrm{e}^{-\mathrm{Pe}}$. In streaming potential measurements, concentration polarization develops to an extent determined by the Peclet number.

We consider next an electrolyte flux density $j_\pm > 0$ across the IEM. The electrolyte concentration distribution in the DBLs is

$$\varepsilon j_\pm = -D_{12}\frac{\mathrm{d}c}{\mathrm{d}x} + c\varepsilon v \rightarrow \mathrm{d}\ln\left(c - j_\pm/v\right) = (\mathrm{Pe}/\delta)\mathrm{d}x \tag{29}$$

$$c(x) = \frac{j_\pm}{v} + \left(c^{\mathrm{b}} - \frac{j_\pm}{v}\right)\exp\left[\frac{x+\delta}{\delta}\mathrm{Pe}\right] \geq c^{\mathrm{b}}, \quad -\delta \leq x \leq 0 \tag{30}$$

$$c(x) = \frac{j_\pm}{v} + \left(c^{\mathrm{b}} - \frac{j_\pm}{v}\right)\exp\left[-\frac{L+\delta-x}{\delta}\mathrm{Pe}\right] \leq c^{\mathrm{b}},\ L \leq x \leq L+\delta\,, \tag{31}$$

where we have used $j_\pm \leq vc^{\mathrm{b}}$, a reasonable assumption because the electrolyte flux density across the IEM with no concentration difference in the external solutions is small. The concentrations at the external membrane boundaries are

$$\frac{c(0)}{c^{\mathrm{b}}} = \frac{j_\pm}{vc^{\mathrm{b}}} + \left(1 - \frac{j_\pm}{vc^{\mathrm{b}}}\right)\mathrm{e}^{\mathrm{Pe}} \approx 1 + \left(1 - \frac{j_\pm}{vc^{\mathrm{b}}}\right)\mathrm{Pe}\,, \tag{32}$$

$$\frac{c(L)}{c^{\mathrm{b}}} = \frac{j_\pm}{vc^{\mathrm{b}}} + \left(1 - \frac{j_\pm}{vc^{\mathrm{b}}}\right)\mathrm{e}^{-\mathrm{Pe}} \approx 1 - \left(1 - \frac{j_\pm}{vc^{\mathrm{b}}}\right)\mathrm{Pe}\,, \tag{33}$$

where the approximations are valid only when $\mathrm{Pe} \ll 1$.

In the IEM, the equations for the ion flux densities are

$$j_\pm = -D_1\left(\frac{\mathrm{d}c_2}{\mathrm{d}x} + z_1c_1f\frac{\mathrm{d}V}{\mathrm{d}x}\right) + c_1v\,, \tag{34}$$

$$j_\pm = -D_2\left(\frac{\mathrm{d}c_2}{\mathrm{d}x} + z_2c_2f\frac{\mathrm{d}V}{\mathrm{d}x}\right) + c_2v\,. \tag{35}$$

For a symmetric electrolyte $c_1 = c_2 + X$, and Eqs. 34 and 35 imply

$$\frac{\mathrm{d}V}{\mathrm{d}x} = \frac{1}{z_1 f\left(D_1 c_1 + D_2 c_2\right)}\left[\left(D_2 - D_1\right)\frac{\mathrm{d}c_2}{\mathrm{d}x} + Xv\right], \tag{36}$$

$$j_\pm = -D_{12}^{\mathrm{M}}\frac{\mathrm{d}c_2}{\mathrm{d}x} + \frac{2D_{12}^{\mathrm{M}}}{D_{12}}\frac{c_1 c_2}{c_1 + c_2}v\,, \tag{37}$$

where $D_{12}^{\mathrm{M}} = D_1 D_2\left(c_1 + c_2\right)/\left(D_1 c_1 + D_2 c_2\right)$ is the electrolyte diffusion coefficient in the IEM.[8] Assuming further that $D_1 = D_2$, the diffusion potential vanishes, and Eqs. 36 and 37 simplify to

$$\frac{\mathrm{d}V}{\mathrm{d}x} = \frac{Xv}{z_1 f D\left(c_1 + c_2\right)}\,, \tag{38}$$

$$j_\pm = -D\frac{\mathrm{d}c_2}{\mathrm{d}x} + \frac{2c_1 c_2}{c_1 + c_2}v\,. \tag{39}$$

For strongly-charged IEMs, $c_1 = c_2 + X \gg c_2$, Eq. 39 reduces to

$$j_\pm = -D\frac{\mathrm{d}c_2}{\mathrm{d}x} + 2c_2 v\,. \tag{40}$$

The solution of Eq. 40 is

$$c_2(x) = c_2(0) + \left[c_2(L) - c_2(0)\right]\frac{\mathrm{e}^{2vx/D} - 1}{\mathrm{e}^{2vL/D} - 1} \tag{41}$$

$$\frac{j_\pm}{2v} = c_2(0) + \frac{c_2(0) - c_2(L)}{\mathrm{e}^{2\mathrm{Pe}^{\mathrm{M}}} - 1}\,, \tag{42}$$

where we have used $2vL/D = 2\mathrm{Pe}^{\mathrm{M}}$ because $D_{12} = D$. Note that $\mathrm{Pe} = \varepsilon v\delta/D_{12}$ and $\mathrm{Pe}^{\mathrm{M}} \equiv vL/D = \mathrm{Pe}\,L/\varepsilon\delta$ are the Peclet numbers in the DBLs and in the membrane. Typically, $L/\varepsilon\delta$ is larger than unity so that the effect of convection on the concentration distribution is typically more important inside the membrane. Thus, for instance, if $2vL/D \gg 1$ then the co-ion concentration is $c_2(x) \approx c_2(0)$ for most of the membrane thickness, except for a region close to the low-pressure interface.

In strongly-charged membranes, the co-ion concentrations at the internal boundaries

satisfy

$$\frac{c_2(0)}{c^{\mathrm{b}}} \approx \frac{c^{\mathrm{b}}}{X}\left(\frac{c(0)}{c^{\mathrm{b}}}\right)^2 \approx \frac{c^{\mathrm{b}}}{X}\mathrm{e}^{\mathrm{Pe}}\left[\mathrm{e}^{\mathrm{Pe}} + 2\left(1-\mathrm{e}^{\mathrm{Pe}}\right)\frac{j_\pm}{c^{\mathrm{b}}v}\right], \tag{43}$$

$$\frac{c_2(L)}{c^{\mathrm{b}}} \approx \frac{c^{\mathrm{b}}}{X}\left(\frac{c(L)}{c^{\mathrm{b}}}\right)^2 \approx \frac{c^{\mathrm{b}}}{X}\mathrm{e}^{-\mathrm{Pe}}\left[\mathrm{e}^{-\mathrm{Pe}} + 2\left(1-\mathrm{e}^{-\mathrm{Pe}}\right)\frac{j_\pm}{c^{\mathrm{b}}v}\right]. \tag{44}$$

From Eqs. 42−44 these concentrations and the electrolyte flux density can be evaluated as

$$\frac{j_\pm}{vc^{\mathrm{b}}} = 2\frac{c^{\mathrm{b}}}{X}\mathrm{e}^{2\mathrm{Pe}}\left[1+\frac{1-\mathrm{e}^{-4\mathrm{Pe}}}{\mathrm{e}^{2\mathrm{Pe}^{\mathrm{M}}}-1}\right] \approx 2\frac{c^{\mathrm{b}}}{X}\mathrm{e}^{2\mathrm{Pe}}, \tag{45}$$

$$\frac{c_2(0)}{c^{\mathrm{b}}} \approx \frac{c^{\mathrm{b}}}{X}\mathrm{e}^{2\mathrm{Pe}}\left[1+4\mathrm{e}^{\mathrm{Pe}}\left(1-\mathrm{e}^{\mathrm{Pe}}\right)\frac{c^{\mathrm{b}}}{X}\right], \tag{46}$$

$$\frac{c_2(L)}{c^{\mathrm{b}}} \approx \frac{c^{\mathrm{b}}}{X}\mathrm{e}^{-2\mathrm{Pe}}\left[1-4\mathrm{e}^{2\mathrm{Pe}}\left(1-\mathrm{e}^{\mathrm{Pe}}\right)\frac{c^{\mathrm{b}}}{X}\right]. \tag{47}$$

In conclusion, concentration polarization develops during streaming potential measurements. These remarks estimate its order of magnitude and provide some insights into the effect of the membrane thickness. Our experimental setup provides reasonably accurate streaming potential measurements, despite the concentration polarization, because the applied pressure is varied cyclically and compensation occurs, although hysteresis is noticeable in the thicker membranes.

References

(1) Cervera, J.; Manzanares, J. A.; Mafé, S. Ion size effects on the streaming potential of narrow charged pores. *Phys. Chem. Chem. Phys.* **2001**, *3*, 2493–2496.

(2) Brun, T.; Vaula, D. Correlation of measurements of electroosmosis and streaming potentials in ion exchanger membranes. *Ber. Bunsenges. Phys. Chem.* **1967**, *71*, 824–829.

(3) Westermann-Clark, G.; Anderson, J. Experimental verification of the space-charge model

for electrokinetics in charged microporous membranes. *J. Electrochem. Soc.* **1983**, *130*, 839–847.

(4) Cervera, J.; García-Morales, V.; Pellicer, J. Ion size effects on the electrokinetic flow in nanoporous membranes caused by concentration gradients. *J. Phys. Chem. B* **2003**, *107*, 8300–8309.

(5) Mafé, S.; Manzanares, J.; Pellicer, J. On the introduction of the pore wall charge in the space-charge model for microporous membranes. *J. Membr. Sci.* **1990**, *51*, 161–168.

(6) Manzanares, J. A.; Mafé, S.; Ramírez, P. Pore conductivity and streaming potential in charged capillary tubes with concentration dependent pore wall charge. *J. Non-Equilib. Thermodyn.* **1991**, *16*, 255–265.

(7) Kontturi, K.; Savonen, A.; Vuoristo, M.; Volden, H. V.; Wang, D.-N.; Paulsen, G. B.; Nielsen, R. I.; Olsen, C. E.; Pedersen, C.; Stidsen, C. E. Study of adsorption and ion-exchange properties of some porous membranes. *Acta Chem. Scand.* **1994**, *48*, 1–11.

(8) Kontturi, K. K.; Murtomäki, L.; Manzanares, J. A. *Ionic Transport Processes: in Electrochemistry and Membrane Science*; Oxford University Press, 2015; pp 163,167 ff.,205 ff.

(9) Toyoshima, Y.; Nozaki, H. Streaming potential across a charged membrane. *J. Phys. Chem.* **1969**, *73*, 2134–2141.